

but unfortunately did not result in the resolution of hyperfine structure. It is conceivable that strain broadening^{22,23} is significant for the nickel-oxime crystal, in which case operation at a lower microwave frequency²² might improve the resolution.

Note Added in Proof. Shortly after acceptance of this paper for publication, a complete X-ray diffraction study of both Ni(II) and

Ni(IV) complexes appeared in the literature.²⁴ N-N direction cosines computed from the data for the Ni(IV) complex agree reasonably well with those given in our Table II when allowance is made for the difference in numerical labeling of the ligand nitrogens.

Registry No. [Ni^{IV}L](ClO₄)₂, 55188-34-6; [NiHL](ClO₄)₂, 55894-12-8.

(22) Froncisz, W.; Hyde, J. S. *J. Chem. Phys.* **1980**, *73*, 3123.

(23) Hagen, W. R. *J. Magn. Reson.* **1981**, *44*, 447.

(24) Korvenranta, J.; Saarinen, H.; Näsäkkälä, M. *Inorg. Chem.* **1982**, *21*, 4296.

Contribution from the Department of Chemistry,
Indian Institute of Technology, Madras 600 036, India

Structural and Magnetic Investigations on the CT Ion-Radical Salt (*p*-(Dimethylamino)phenyl)dimethylammonium Bis(maleonitriledithiolato)nickelate(III)

B. L. RAMAKRISHNA and P. T. MANOHARAN*

Received February 25, 1982

A detailed study of (TMPD)Ni(mnt)₂ by a variety of physical methods—X-ray crystallography, electronic absorption spectroscopy, magnetic susceptibility, electrical conductivity, and EPR—has been carried out. Though Ni(mnt)₂⁻ and TMPD⁺ form segregated stacks along the "a" axis in the triclinic modification P $\bar{1}$, a number of short contacts between the units facilitate charge transfer from TMPD⁺ to Ni(mnt)₂⁻. Both susceptibility and EPR studies indicate two temperature regions, $T < 100$ K and $T > 100$ K. In the $T < 100$ K region, where the behavior is Curie-Weiss type, the decomposition of total susceptibility shows that at 4.2 K about 90% of the contribution comes from the Ni(mnt)₂⁻ stack. A value of exchange (~ 120 cm⁻¹) has been found from the dependence of χ on temperature in the $T > 100$ K region. Powder EPR studies yielded a ratio of D_e/J to be 1.94×10^{-2} . Single-crystal EPR studies at 77 K clearly indicate a change in the principal axis cosines and from line width analysis in the plane perpendicular to "a" give the best fit for $J = -6.5$ cm⁻¹, $D_e = -0.13$ cm⁻¹, and $\rho = 5$. The line shape analysis shows low-dimensional behavior for $B \parallel a$ and nearly Lorentzian behavior for $B \perp a$.

1. Introduction

Recently, considerable interest has been focused on crystalline solids with the gross anisotropy of at least one intensive variable such as conductivity, magnetic susceptibility, etc.¹⁻³ These variations are associated with a columnar crystallographic packing, and perhaps the best examples of these are based on TCNQ⁻ ion-radical salts.^{4,5}

Platelike transition-metal complexes which stack as columnar structures provide a chemically flexible class of such materials.⁶ Maleonitriledithiolene metal complexes⁷ [M(mnt)₂]ⁿ⁻ are a well-studied class of coordination compounds which possess an overall planar geometry irrespective of the metal or its oxidation state. These undergo facile reversible electron-transfer reactions, have highly delocalized electronic structures, and are known for their ability to form donor-acceptor compounds with organic donor molecules⁸⁻¹⁶ to give

a D⁺A⁻ salt where D⁺ and/or A⁻ are paramagnetic.

In our effort to characterize new examples of quasi-1-D systems, we have synthesized and studied a new crystalline ion-radical salt, (*p*-(dimethylamino)phenyl)dimethylammonium (maleonitriledithiolato)nickelate(III) (TMPD⁺Ni(mnt)₂⁻), shown in Figure 1.

We report here a detailed study of TMPD⁺Ni(mnt)₂⁻ by a variety of physical methods—crystallography, electronic absorption spectroscopy, magnetic susceptibility, electrical conductivity, and electron paramagnetic resonance. Both the TMPD⁺ and the Ni(mnt)₂⁻ moieties are $S = 1/2$ systems, are planar, and have highly delocalized electronic structures. Thus, TMPD⁺Ni(mnt)₂⁻ combines the advantages of the infinite variety of organic compounds with the electronic structural flexibility of the transition-metal complexes.

Our X-ray structure (section 3A) shows that the TMPD⁺ ions and the Ni(mnt)₂⁻ ions stack among themselves, forming segregated regular stacks. Though static susceptibility (section 3D) measurements yield interesting information, single-crystal EPR results (section 3E) yield a surprisingly detailed picture of the magnetic phenomena.

This compound has advantages over other similar compounds studied earlier on two counts, detailed crystal and molecular structural data and single-crystal EPR information. Though magnetic data^{10,12-13} are available on compounds such as (phenothiazine)⁺Ni(thiete)₂⁻, TTF⁺Ni(mnt)₂⁻, and (perylene)₂⁺Pd(mnt)₂⁻, crystal and molecular structural information is lacking. Despite a knowledge of the detailed molecular structures^{16,17} of ion-radical salts such as TTF⁺Pt(thiete)₂⁻ and TTF⁺Ni(thiete)₂⁻ large EPR line widths of the

(1) Keller, H. J., Ed. "Low Dimensional Cooperative Phenomena"; Plenum Press: New York, 1975.

(2) Keller, H. J., Ed. "Chemistry and Physics of 1d metals"; Plenum Press: New York, 1977.

(3) Soos, Z. G. *Annu. Rev. Phys. Chem.* **1974**, *25*, 121.

(4) Shchegolev, I. F. *Phys. Status Solidi A* **1972**, *12*, 9.

(5) Garito, A. F.; Heeger, A. J. *Acc. Chem. Res.* **1974**, *7*, 232.

(6) Miller, J. S.; Epstein, A. J. *Prog. Inorg. Chem.* **1976**, *20*, 1.

(7) McCleverty, J. A. *Prog. Inorg. Chem.* **1968**, *10*, 49.

(8) Schmitt, R. D.; Wing, R. M.; Maki, A. H. *J. Am. Chem. Soc.* **1969**, *91*, 4394.

(9) Wing, R. M.; Schlupp, R. L. *Inorg. Chem.* **1970**, *9*, 471.

(10) Geiger, W. E.; Maki, A. H. *J. Phys. Chem.* **1971**, *75*, 2387.

(11) Hove, M. J.; Hoffman, B. M.; Ibers, J. A. *J. Chem. Phys.* **1972**, *56*, 3490.

(12) Wudl, F.; Ho, C. H.; Nagel, A. *J. Chem. Soc., Chem. Commun.* **1973**, 923.

(13) Alcacer, L.; Maki, A. H. *J. Phys. Chem.* **1974**, *78*, 215.

(14) Jacobs, I. S.; Bray, J. W.; Hart, H. R., Jr.; Interrante, L. V.; Kasper, J. S.; Watkins, G. O.; Prober, D. E.; Banner, J. C. *Phys. Rev. B: Solid State* **1976**, *14*, 3036.

(15) Interrante, L. V.; Bray, J. W.; Hart, H. R., Jr.; Kasper, J. S.; Piacente, P. A. *J. Am. Chem. Soc.* **1977**, *99*, 3523.

(16) Bonner, J. C.; Wei, T. S.; Hart, H. R., Jr.; Interrante, L. V.; Jacobs, I. S.; Kasper, J. S.; Watkins, G. D.; Blofe, H. W. *J. Appl. Phys.* **1978**, *49*, 1321.

(17) Jacobs, I. S.; Interrante, L. V.; Hart, H. R., Jr. *AIP Conf. Proc.* **1975**, *No. 24*, 355.

Table I. Fractional Positional Coordinates ($\times 10^4$) and Anisotropic Thermal Parameters ($\times 10^4$) for Non-Hydrogen Atoms^a

| atom | x | y | z | U_{11} | U_{22} | U_{33} | U_{23} | U_{13} | U_{12} |
|----------------|-----------|-----------|-----------|-----------|-----------|-----------|-----------|-----------|----------|
| Ni | 0 | 0 | 0 | 875 (19) | 654 (16) | 613 (15) | 378 (13) | 309 (14) | 282 (14) |
| S ₁ | -1365 (6) | 1055 (5) | 1203 (5) | 474 (24) | 339 (19) | 266 (19) | 205 (17) | 195 (17) | 225 (14) |
| S ₂ | -136 (6) | 2230 (5) | 2469 (5) | 430 (23) | 302 (18) | 256 (18) | 186 (16) | 179 (16) | 190 (17) |
| C ₁ | 1526 (21) | 443 (19) | 3392 (19) | 248 (71) | 319 (72) | 274 (73) | 202 (63) | 144 (60) | 75 (59) |
| C ₂ | 842 (20) | 1804 (17) | 3869 (18) | 247 (69) | 219 (62) | 198 (65) | 87 (54) | 117 (55) | 31 (53) |
| C ₃ | 2325 (24) | 91 (20) | 4571 (20) | 465 (92) | 364 (76) | 222 (70) | 232 (66) | 153 (66) | 198 (69) |
| C ₄ | 986 (27) | 3084 (21) | 5712 (20) | 520 (98) | 348 (80) | 199 (72) | 125 (66) | 163 (69) | 171 (74) |
| N ₁ | 1216 (26) | 4100 (20) | 7213 (20) | 622 (102) | 449 (85) | 396 (83) | 222 (73) | 263 (76) | 199 (76) |
| N ₂ | 7042 (25) | 140 (20) | 4428 (22) | 637 (102) | 463 (82) | 493 (89) | 324 (76) | 328 (81) | 236 (75) |
| N ₃ | 6148 (20) | 5771 (18) | 8235 (17) | 341 (73) | 460 (77) | 240 (66) | 205 (60) | 79 (54) | 43 (50) |
| C ₅ | 7051 (31) | 4665 (28) | 8575 (28) | 593 (105) | 656 (110) | 608 (110) | 507 (105) | 290 (101) | 305 (99) |
| C ₆ | 5627 (24) | 5428 (20) | 6740 (21) | 378 (85) | 296 (72) | 284 (79) | 180 (63) | 160 (65) | 65 (62) |
| C ₇ | 5796 (31) | 7385 (27) | 9866 (24) | 568 (109) | 575 (106) | 328 (91) | 191 (87) | 230 (27) | 7 (80) |
| C ₈ | 5847 (21) | 3876 (19) | 5177 (20) | 220 (69) | 317 (70) | 321 (80) | 210 (65) | 72 (52) | 77 (52) |
| C ₉ | 5332 (23) | 3508 (20) | 3655 (22) | 299 (77) | 320 (73) | 347 (81) | 188 (66) | 180 (63) | 126 (59) |

^a Standard deviations in the last digits are in parentheses.

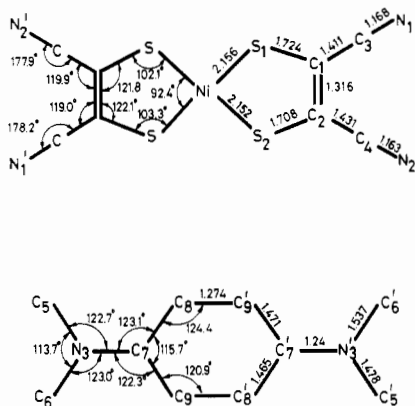


Figure 1. Bond lengths and bond angles of the $\text{Ni}(\text{mnt})_2^-$ and TMPD^+ units in the ion-radical salt.

order of several hundred gauss even at low temperatures have resulted in the absence of detailed magnetic data. For at least two compounds^{11,18} $-(\text{TMPD}^+)_2\text{Ni}(\text{mnt})_2^-$ and $\text{C}_7\text{H}_7^+\text{Ni}(\text{mnt})_2^-$ —detailed magnetic and crystal structure information is available but they are different from our system in that only one of the component ions is paramagnetic.

2. Experimental Section

A. Preparation. $\text{TMPD}^+\text{ClO}_4^-$ and $[\text{N}(\text{C}_2\text{H}_5)_4]^+\text{Ni}(\text{mnt})_2^-$ were prepared by methods described in the literature.¹⁹⁻²⁰ A boiling solution of 146 mg of $[\text{N}(\text{C}_2\text{H}_5)_4]^+\text{Ni}(\text{mnt})_2^-$ in 50 mL of acetone was added to a boiling solution of 100 mg of $\text{TMPD}^+\text{ClO}_4^-$ in 200 mL of acetone all at once. When the solution was allowed to evaporate slowly, violet-black shining needlelike crystals were deposited in very poor yield. Pure crystals were carefully chosen for the purpose of EPR measurement. Anal. Calcd for $\text{TMPD}^+\text{Ni}(\text{mnt})_2^-$: C, 42.93; N, 16.70; H, 3.18. Found: C, 42.74; N, 16.23; H, 3.26. However, powder samples could be made in large yield as has been reported by Miles and Wilson.²¹

B. Determination of the Crystal Structure. (i) **Unit Cell and Space Group.** A crystal of $0.5 \times 0.1 \times 0.8 \text{ mm}^3$ dimension was mounted on an Enraf-Nonius four-circle automatic diffractometer. The unit cell parameters were obtained from a least-squares calculation of 15 centered reflections. These centered reflections were collected with use of $\text{Mo K}\alpha$ (0.7093 Å) radiation monochromatized from the (002) plane of a graphite monochromator. The Delaunay reduced cell parameters were determined to be as follows: $a = 7.334 \text{ Å}$; $\alpha = 128.00^\circ$; $b = 9.956 \text{ Å}$; $\beta = 108.08^\circ$; $c = 10.269 \text{ Å}$; $\gamma = 92.06^\circ$; $V = 535.3 \text{ Å}^3$; $\rho = 1.56 \text{ g cm}^{-3}$; $Z = 1$. The formula weight is 503 g mol^{-1} , and the calculated linear absorption coefficient is $\mu = 13.4 \text{ cm}^{-1}$.

(ii) **Collection and Reduction of Data.** The intensity data were collected with the monochromatized $\text{Mo K}\alpha$ radiation in the range $2^\circ < \theta < 30^\circ$ with use of a moving-crystal, moving-goniometer scan technique. The quality of the crystal was checked by using the open counter ω -scan technique for a few reflections. The high value of the average peak width at half-height implies high mosaicity in the crystal. Intensities were measured by using the $\omega/2\theta$ scan technique with variable scan speed. The scan width for each reflection was $(0.85 + 0.35 \tan \theta)^\circ$, and the background was scanned on either side of the peak for 25% of this value. Very strong reflections with counts more than 50 000 counts s^{-1} were attenuated by a zirconium filter in the diffracted beam. Two strong reflections were used as standard and were measured after every 100 min to check the stability of the instrument and the crystal.

Out of a possible 2887 reflections in the Mo sphere, 1710 were observed as strong reflections with $F_o^2 > 3\sigma(F_o^2)$. These 1710 reflections were corrected for Lorentz and polarization effects by multiplying the intensity by $1/Lp$, which is given by

$$\frac{(\sin 2\theta)(1 + \cos 2\theta_m)}{\cos 2\theta_m + \cos^2 2\theta}$$

where θ is the Bragg angle of the reflection and θ_m is the Bragg angle of the reflecting plane of the monochromator ($\theta_m = 6.1^\circ$ for $\text{Mo K}\alpha$), and were used without absorption corrections for further structure analysis.

(iii) **Solution and Refinement of the Structure.** The data were collected with a CAD-4 diffractometer with $\text{Mo K}\alpha$ radiation. The structure was solved by using the heavy-atom method. Details are in Appendix A. The positional and thermal parameters of the non-hydrogen atoms are given in Table I.

Since Wilson's statistics indicated the presence of a center of symmetry, a $P\bar{1}$ space group was assumed and the reasonableness of the final structure justifies this assumption.

C. Magnetic Susceptibility Measurements. Preliminary magnetic susceptibility measurements were done at the Solid State and Structural Chemistry Unit of the IIS, Bangalore, India, in the temperature range 120–360 K with a Faraday balance. The low-temperature results down to 4 K were obtained for every 0.5° interval from the laboratory of Dr. T. O. Poehler, University of Maryland.

D. Electron Paramagnetic Resonance. Experiments were performed with Varian Associates E-4 and E-112 X- and Q-band spectrometers with 100-kHz modulation. The temperature dependence has been studied from 4 to 300 K. DPPH was used as a g calibrator. From the angular variation of the resonance line of a single crystal, the principal components and their direction cosines were obtained with use of the usual diagonalization procedures. The undiagonalized g matrix was formed by a least-squares fit of the angular variation in three orthogonal planes. By a transformation the orientation of the magnetic tensor principal axes with respect to the molecular framework is obtained.

E. IR and Optical Measurements. Polycrystalline and solution spectra at 300 K were recorded on the DMR-21 spectrophotometer. IR spectra were recorded on a Perkin-Elmer 257 instrument.

F. Electrical Conductivity. A GR 1644-A bridge with a variable-temperature Dewar was used for conductivity measurements down to 77 K.

(18) Manoharan, P. T.; Noordik, J. H.; de Boer, E.; Keijzers, C. P. *J. Chem. Phys.* **1981**, *74*, 1981.

(19) Michalis, L.; Granick, S. *J. Am. Chem. Soc.* **1943**, *65*, 1741.

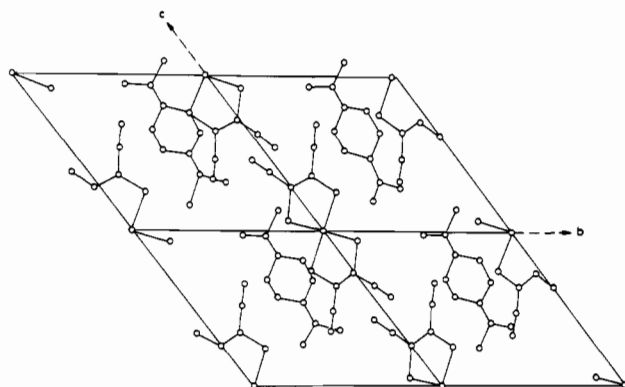
(20) Davison, A.; Edelstein, N.; Holm, R. H.; Maki, A. H. *Inorg. Chem.* **1963**, *2*, 1227.

(21) Miles, M. G.; Wilson, J. D. *Inorg. Chem.* **1975**, *14*, 2357.

Table II. Weighted Least-Squares Planes for Ni(mnt)₂⁻ and TMPD⁺

| Plane Equation: $Ax + By + Cz + D = 0^a$ | | | | | |
|--|--------|-----------------|---------|-----------------|-----|
| | A | B | C | D | |
| plane 1 | 6.2385 | 4.0001 | -3.3063 | -2.9192 | |
| plane 2 | 6.1847 | 3.9541 | -3.0557 | -3.5674 | |
| Deviations from Planarity (10^{-3} Å) | | | | | |
| atom | dev | atom | dev | atom | dev |
| Plane 1 | | | | | |
| Ni | 13 | C ₁ | 20 | C ₄ | -26 |
| S ₁ | -6.7 | C ₂ | -19 | N ₁ | 22 |
| S ₂ | 3.8 | C ₃ | -11 | N ₂ | 11 |
| Plane 2 | | | | | |
| N ₃ | 6.5 | C ₁₀ | -0.5 | C ₁₂ | -12 |
| C ₉ | -0.5 | C ₁₁ | 5.5 | C ₁₃ | +3 |

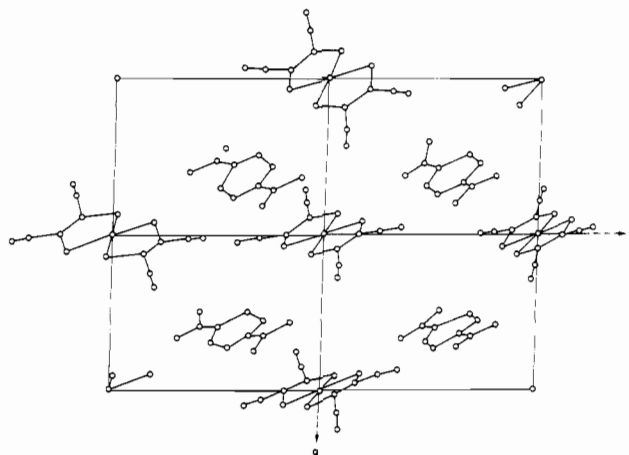
^a x , y , and z are triclinic fractional coordinates. Plane 1 contains a Ni atom, two S atoms, four C atoms, and two N atoms of the Ni(mnt)₂⁻ unit. Plane 2 contains 5 C atoms and a N atom of the TMPD⁺ moiety.

Figure 2. Projection of the structure of (TMPD)Ni(mnt)₂ down the "a" axis, showing short contacts between the two moieties.

3. Results and Discussion

A. Description of the Structure. The bond distances and bond angles of the two moieties, TMPD⁺ and Ni(mnt)₂⁻, are shown in Figure 1. Both the Ni(mnt)₂⁻ ion centered at (0, 0, 0) and the TMPD⁺ ion centered at (1/2, 1/2, 1/2) possess a center of symmetry and exhibit a nearly planar structure. The equations of the least-squares plane through the anion and cation are given in Table II. As is seen from the table, the Ni(mnt)₂⁻ and TMPD⁺ planes are both very nearly parallel. They form uniformly spaced, segregated stacks in the crystal, the stacking axis being the crystallographic "a" axis. The projections down the *a* and *c* axes are shown in Figures 2 and 3, respectively. Even though the two ions form segregated stacks and there is no lateral overlap of the two planes, there are numerous short interatomic contact distances along the long edges of the two molecules. The cyanide and sulfur groups of Ni(mnt)₂⁻ and the nitrogen atoms of TMPD⁺ are particularly close (3.4 Å). Table III lists the contact distances below 4.2 Å between various atoms in the two moieties. In Table IV a comparison of some of the anion bond distances in N(C₂H₅)₄Ni^{III}(mnt)₂, (TMPD)₂Ni^{II}(mnt)₂, and (TMPD)Ni^{III}(mnt)₂ are given. Table V gives a comparison of bond lengths in the cation unit TMPD⁺ in various TMPD compounds.

The Ni-S bond length of 2.152 (4) Å is typical of Ni^{III}-S bonds and compares well with N(C₂H₅)₄Ni(mnt)₂. The cyanide bond length is very sensitive to the changes in the metal oxidation state or in general to the total electron density in the anion unit. In our case we find that the cyanide bond length is by far the largest found in Ni²⁺ and Ni³⁺ compounds

Figure 3. Projection of the structure of (TMPD)Ni(mnt)₂ down the "c" axis, showing the Ni(mnt)₂⁻ and TMPD⁺ stack along "a".Table III. Some Short Contact Distances (Å) between Various Atoms of the Two Moieties TMPD⁺ and Ni(mnt)₂⁻

| | | | |
|--------------------------------|------|--------------------------------|------|
| Ni-N ₃ | 3.93 | Ni-C ₆ | 3.88 |
| Ni-C ₇ | 3.95 | | |
| S ₁ -C ₅ | 3.85 | S ₂ -N ₃ | 3.95 |
| S ₁ -C ₆ | 3.93 | S ₂ -C ₆ | 4.18 |
| S ₁ -S ₈ | 4.19 | S ₂ -C ₇ | 3.53 |
| S ₁ -C ₉ | 3.99 | S ₂ -C ₈ | 3.69 |
| | | S ₂ -C ₉ | 3.97 |
| C ₁ -C ₈ | 3.61 | C ₁ -C ₉ | 3.88 |
| C ₂ -C ₇ | 3.71 | C ₂ -C ₉ | 3.78 |
| C ₃ -C ₈ | 4.06 | C ₃ -C ₅ | 4.06 |
| C ₄ -C ₆ | 3.98 | C ₄ -C ₈ | 3.87 |
| C ₄ -C ₇ | 3.49 | | |
| N ₁ -N ₃ | 3.46 | N ₂ -C ₅ | 3.83 |
| N ₁ -C ₅ | 3.46 | N ₂ -C ₆ | 3.44 |
| N ₁ -C ₇ | 3.71 | N ₂ -C ₈ | 3.50 |
| N ₁ -C ₉ | 4.04 | N ₂ -C ₉ | 4.04 |

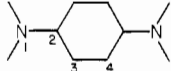
Table IV. Comparison of Bond Lengths (Å) in the Anions of N(C₂H₅)₄Ni^{III}(mnt)₂,^a (TMPD)₂Ni^{II}(mnt)₂,^b and (TMPD)Ni^{III}(mnt)₂.^c

| bond | N(C ₂ H ₅) ₄ Ni ^{III} (mnt) ₂ | | |
|--------------------------------|---|--|--|
| | (TMPD) ₂ Ni ^{II} (mnt) ₂ | (TMPD)Ni ^{III} (mnt) ₂ | (TMPD)Ni ^{III} (mnt) ₂ |
| Ni-S ₁ | 2.144 (2) | 2.173 (2) | 2.152 (4) |
| S ₁ -C ₁ | 1.719 (9) | 1.731 (5) | 1.708 (15) |
| C ₁ -C ₂ | 1.359 (12) | 1.379 (6) | 1.315 (18) |
| C ₁ -C ₃ | 1.437 (13) | 1.414 (7) | 1.431 (18) |
| C ₃ -N ₁ | 1.125 (13) | 1.148 (6) | 1.155 (12) |

^a Our work (unpublished) and also: Sasaki, Y.; Kobayashi, A. *Bull. Chem. Soc. Jpn.* 1977, 50, 2650. ^b Reference 11. ^c Present work.

(Table IV). We find a value of 1.155 (12) Å, which is large compared to 1.125 (13) Å in N(C₂H₅)₄Ni^{III}(mnt)₂ and is closer to that in the Ni^{II} compound (TMPD)₂Ni(mnt)₂, where it is found to be 1.148 (6) Å. This along with the fact that there are several short contact distances between the CN group of Ni(mnt)₂⁻ and the TMPD⁺ unit indicates that there has been some electron transfer from TMPD⁺ to Ni(mnt)₂⁻.

This is further confirmed by the very pronounced quinonoid structure found in the TMPD⁺ unit of this compound as compared to that in other TMPD compounds (Table VI). The bond distances are much closer to TMPD²⁺ rather than TMPD⁺, indicating that it has acquired more than a single

Table V. Comparison of the Bond Lengths (Å) in the TMPD⁺ Moiety of Some Compounds of TMPD⁺


| compd | R_{12} | R_{23} | R_{34} | ref |
|---|------------|------------|------------|-----------|
| TMPD ⁺ ClO ₄ ⁻ | 1.346 (2) | 1.426 (3) | 1.365 (6) | <i>a</i> |
| (TMPD)TCNQ | 1.365 (7) | 1.416 (7) | 1.374 (10) | <i>b</i> |
| (TMPD)chloranil | 1.357 | 1.405 | 1.374 | <i>c</i> |
| (TMPD) ₂ Ni(mnt) ₂ | 1.352 (6) | 1.424 (6) | 1.344 (6) | <i>d</i> |
| TMPD ²⁺ | 1.309 | 1.456 | 1.322 | <i>e</i> |
| (TMPD)Ni(mnt) ₂ | 1.265 (30) | 1.454 (20) | 1.281 (25) | this work |

^a de Boer, J. L.; Vos, A. *Acta Crystallogr., Sect. B* 1972, *B28*, 835. ^b Hanson, A. W. *Acta Crystallogr.* 1965, *19*, 610. ^c de Boer, J. L.; Vos, A. *Acta Crystallogr., Sect. B* 1968, *B24*, 720. ^d Reference 11. ^e Values calculated by using the PPP method by D. Kracht and the results reported in the reference in footnote *a*.

Table VI. Comparison of Optical Spectra of N(C₂H₅)₄Ni(mnt)₂, (TMPD)Ni(mnt)₂, and (TMPD)ClO₄

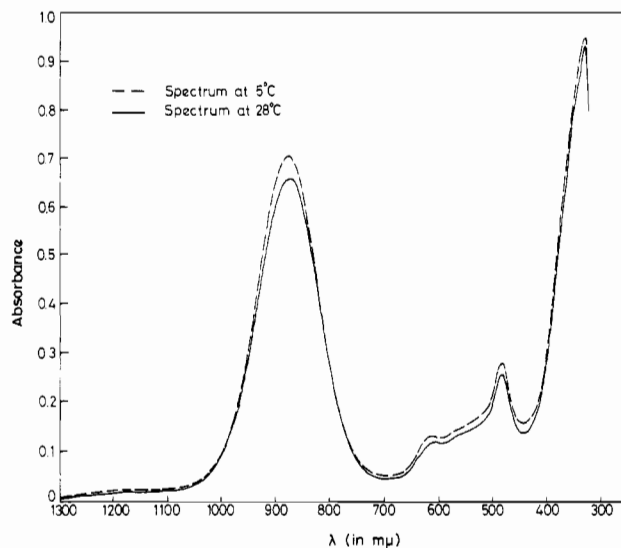
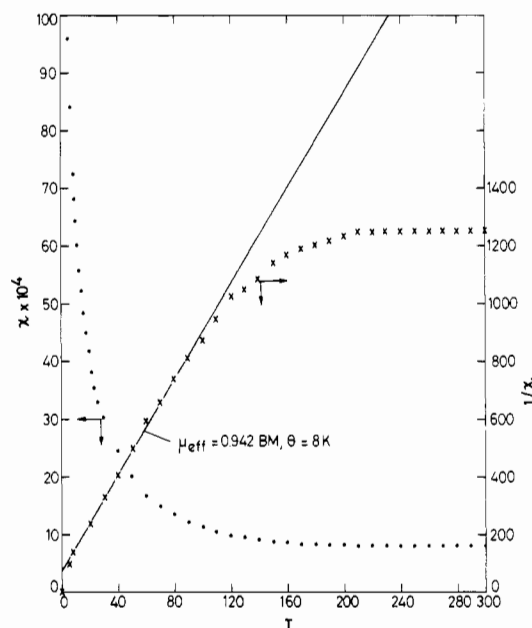
| λ , cm ⁻¹ | intens ^a (ϵ) | half-width at 1/ ϵ of intens, cm ⁻¹ |
|--|------------------------------------|---|
| N(C ₂ H ₅) ₄ Ni(mnt) ₂ ^b | | |
| 11 430 | 0.30 (8000) | 1000 (L π → M) |
| 16 707 | 0.025 (500) | 800 (parity forbidden) |
| 18 630 | 0.0375 (690) | 950 (parity forbidden) |
| 19 785 | 0.032 (530) | 710 |
| 21 250 | 0.10 (2500) | 1100 (L σ → M) |
| 26 300 | 0.50 (3600) | 2000 (L π → M) |
| TMPD ⁺ ClO ₄ ^c | | |
| 16 390 | 0.21 | 625 |
| 17 778 | 0.21 | 850 |
| 19 220 | 0.11 | 990 |
| 20 760 | 0.04 | 1400 |
| 26 770 | 0.07 | 1570 |
| 31 400 | 0.35 | 1300 |
| TMPD ⁺ Ni(mnt) ₂ ⁻ | | |
| 11 420 | 0.23 | 1100 |
| 16 350 | 0.17 | 680 |
| 16 700 | 0.15 | 810 |
| 19 020 | 0.06 | 1930 |
| 20 300 | 0.06 | 1500 |
| 27 310 | 0.09 | 2250 |
| 31 280 | 0.24 | 2420 |

^a The relative intensities are normalized to one. ^b Shupack, S. I.; Billig, F.; Clark, R. J. H.; Williams, R.; Gray, H. B. *J. Am. Chem. Soc.* 1964 *86*, 4594. ^c Hausser, K. H.; Murrel, J. N. *J. Chem. Phys.* 1957, *27*, 500.

positive charge via electron transfer to the Ni(mnt)₂⁻ unit. Thus we have strong structural evidence of charge transfer from the TMPD⁺ unit to Ni(mnt)₂⁻.

B. Optical and Infrared Studies. The infrared spectrum of (TMPD)Ni(mnt)₂ in the solid state contains bands corresponding to both TMPD⁺ and Ni(mnt)₂⁻ moieties, and there is no appreciable shift in the band positions except in the case of the C≡N stretch, which noticeably shifts by 20 cm⁻¹ toward lower energy as compared to that in N(C₂H₅)₄Ni(mnt)₂. This is in accordance with the structural feature of increased C≡N bond distance (vide supra). This has been explained on the basis of charge transfer from the TMPD⁺ to the Ni(mnt)₂⁻ moiety and the movement of the extra electrons to the antibonding orbitals, thus increasing the bond length.

A comparison of the optical spectra in acetone of N(C₂H₅)₄Ni(mnt)₂, (TMPD)ClO₄, and (TMPD)Ni(mnt)₂ is shown in Table VI. A band deconvolution program was used to fit the experimental spectra to get the band positions, half-widths, and relative intensities. The spectrum is primarily a superposition of the two moieties though there are some noticeable changes in the relative intensities and small shifts

**Figure 4.** Optical spectrum of (TMPD)Ni(mnt)₂ in acetone.**Figure 5.** Temperature variation of susceptibility of (TMPD)Ni(mnt)₂. The χ^{-1} vs. T plot shows clearly the two temperature regions $T < 100$ K, where a Curie-Weiss behavior is seen, and $T > 100$ K, where χ is almost temperature independent.

in the band positions. The spectrum of (TMPD)Ni(mnt)₂ is shown in Figure 4.

The relative intensity of the 11.4×10^3 cm⁻¹ transition with respect to that at 26×10^3 cm⁻¹ increases from 0.6 in the case of N(C₂H₅)₄Ni(mnt)₂ to 2.5 in (TMPD)Ni(mnt)₂. With no contribution from TMPD⁺ in this region there must be a new band around 11×10^3 cm⁻¹ to explain the increase in ratio. However, there can be such effects as the relative intensities of the bands of one moiety changing on complexation. The so called charge-transfer bands (L → M type) are more susceptible to changes.

C. Electrical Conductivity. Measurements showed that at 77 K the conductivity was larger (10^{-7} Ω⁻¹ cm⁻¹) than at 300 K (10^{-9} Ω⁻¹ cm⁻¹). This negative temperature coefficient is unusual, and further work on the single crystal is necessary.

D. Magnetic Susceptibility. The plots χ vs. T and χ^{-1} vs. T given in Figure 5 indicate that there are two temperature regions present, and the preliminary analyses for these two regions are presented below. The susceptibility results are also discussed in light of the random-exchange model.

Table VII. Comparison of Effective Magnetic Moments (μ_{eff}) of Some D⁺A⁻ Type Compounds, Where both D⁺ and A⁻ Are Paramagnetic and Have $S = 1/2$ ^a

| case no. | compd | $\mu_{\text{eff}}, \mu_{\text{B}}$ | ref |
|----------|--|------------------------------------|-----------|
| 1 | (perylene) ₂ Ni(mnt) ₂ | 2.2 | 13 |
| 2 | (perylene) ₂ Pd(mnt) ₂ | 1.03 | 13 |
| 3 | (TTF)Ni(thiete) | 2.27 | 17 |
| 4 | (TTF)Pt(thiete) | 2.24 | 17 |
| 5 | (TMPD)Ni(mnt) ₂ | 0.942 | this work |

^a For a strongly coupled triplet ($S = 1$) system $\mu_{\text{eff}} = g\mu_{\text{B}}S^{1/2}(S + 1) = 2.828 \mu_{\text{B}}$. However, for uncoupled spin $\mu_{\text{eff}} = g\mu_{\text{B}}z^{1/2}S(S + 1)$, where z is the number of uncoupled $S = 1/2$ spins; for $z = 2$, $\mu_{\text{eff}} = 2.45 \mu_{\text{B}}$.

(i) Low-Temperature Region (4.2–100 K). The susceptibility in this region could be fit very well to a Curie–Weiss type of behavior where $C = 0.111 \text{ mol}^{-1}$ and $\Theta = 8 \text{ K}$. The μ_{eff} value is calculated to be $0.942 \mu_{\text{B}}$ and is compared with the μ_{eff} 's of other similar compounds in Table VII.

It was concluded that in cases 1, 3, and 4 of Table VII the two spins independently contribute to the susceptibility with not much interaction between the component ions. This Curie type behavior has been observed before in other systems such as (perylene)₂⁺Pd(mnt)₂⁻¹³ and (TMPD⁺)₂Ni(mnt)₂⁻¹¹ and has been explained to be due to disorder and impurity, respectively. In this case, as the crystals are formed during a chemical reaction and are not recrystallized due to difficulties mentioned earlier, there is a strong possibility of disorder in these crystals. The earlier crystal structure analysis (see section 3A) also indicated the presence of a large amount of disorder.

The occurrence of defects in 1-D systems is quite general and leads to drastic consequences in magnetic and transport properties.¹⁹ A misoriented molecule cuts the system into two segments or interrupted strands. These finite chain effects produce divergent susceptibilities associated with the odd length segments. There exist strong exchanges J along the chain within a segment and also weak exchanges ϵJ between the segments. For $kT \gg J$ all the spins are thermally decoupled and none of the exchanges are important. For $J > kT > \epsilon J$, the exchanges J become important but the segments are still decoupled. Thus, a conventional picture of Curie law type divergences arises when $\epsilon = 0$, i.e. when the odd segments remain decoupled. But the more realistic picture of small but finite interactions between the segments splits the degeneracy and suppresses Curie type divergences. The magnitude of the Curie type tail provides an estimate of the concentration "C" of the breaks in the chain, and the $\chi(T)$ data at low temperature can yield a value for ϵ . Unless they order magnetically due to transverse interactions, all 1d antiferromagnetic materials should show small but finite C and ϵ .

The susceptibility in these systems should follow power laws such as

$$\chi(T) = AT^{-\alpha} \quad \text{i.e. } \log \chi(T) = \log A - \alpha \log T \quad (1)$$

α is found to be usually between 0.72 and 0.89 except in NMPTCNQ, where it is 0.58. Figure 6 shows a plot of $\log \chi(T)$ vs. $\log T$, and the slope yields α . From the very low temperature results (<10 K) we find the slope to be 0.397, which is not in the range mentioned above. But the values from 100 to 20 K yield a good straight line with an α value of 0.837, which is more reasonable. Very accurate determinations of χ at reliable temperatures even down to temperatures lower than 4.2 K will greatly enhance the understanding of the system. The value of ϵ has been later determined to be around 0.1 from EPR line width analysis (part (vii)b of section 3E), and the value of C has been estimated to be 0.23 (part (v) of section 3E and Figure 10).

The constant slope of χ^{-1} vs. T in the above temperature range is an indication of localized moments with a constant

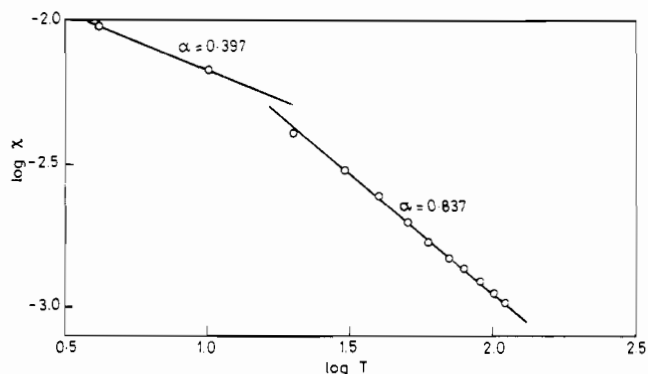


Figure 6. Low-temperature susceptibility in terms of power for $\chi(T) = AT^{-\alpha}$ as derived for a random-exchange Heisenberg antiferromagnetic chain.¹⁹

μ_{eff} . Thus the interpretation in the low-temperature region is that the system is at least partially describable as an ensemble of disordered localized paramagnetic moments. The contribution of these moments to the total χ dominates more and more as the temperature is lowered.

(ii) High-Temperature Region (>100 K). In this region, χ is found to be almost temperature independent, as seen in Figure 5. Several possible explanations may be offered.

(1) Van Vleck type paramagnetism,²² where, in the presence of a magnetic field, an excited state gets mixed with the ground state and gives it a magnetic moment, may be present. This model does not explain a resonance at $g = 2$ and hence can be ruled out.

(2) Pauli spin paramagnetism,²³ which is characteristic of a degenerate electron gas, may exist. A similar temperature-independent paramagnetism is observed in many conducting TCNQ complexes, in particular, for (NMP)TCNQ²⁴ and (quinolinium)(TCNQ)₂.²⁵ But as the room-temperature (300 K) conductivity, $10^{-9} \Omega^{-1}$, measured in this laboratory for a pellet is in good agreement with an earlier report,²¹ this possibility is also ruled out.

(3) The weak temperature dependence of χ can also be well explained by a Heisenberg Hamiltonian with uniform antiferromagnetic interaction. Thus, it can be both a weak Curie type and the uniform antiferromagnetic interactions contributing to susceptibility at high temperatures as has been shown¹³ in a closely related compound, (perylene)₂⁺Pd(mnt)₂⁻.

The last possibility above seems the most reasonable and is also in agreement with the crystal structure in assuming a uniform antiferromagnetic interaction. However, a plot of $\log \chi(T)$ vs. T^{-1} in this high-temperature region is found to be nearly linear and from the slope one can get an energy of activation for magnetism of 126.3 cm^{-1} (0.016 eV). Though one does not expect an activated behavior for segregated regular chain compounds, the above value does give an approximate estimate of the exchange interaction. Further analysis of the magnetic properties is possible only in conjunction with the EPR results, which are discussed in the next section.

E. Electron Paramagnetic Resonance. (i) Solution Data. The acetone solution of the ion-radical salt at 300 K shows two resonances corresponding to TMPD⁺ and Ni(mnt)₂⁻ at $g = 2.003$ and 2.066 , respectively. These agree very well with the g_{av} of the isolated species, indicating that the complex dissociates into solvent-separated ions in solution. However,

(22) Van Vleck, J. H. "Electric and Magnetic Susceptibility"; Oxford University Press: London, 1932; p 145.

(23) Ziman, J. M. "Principles of the Theory of Solids"; Oxford University Press: London, 1969; p 286.

(24) Epstein, A. J.; Eternad, S.; Garito, A. F.; Heeger, A. J. *Phys. Rev. B: Solid State* **1972**, *5*, 952.

(25) Kepler, R. G. *J. Chem. Phys.* **1963**, *39*, 3528.

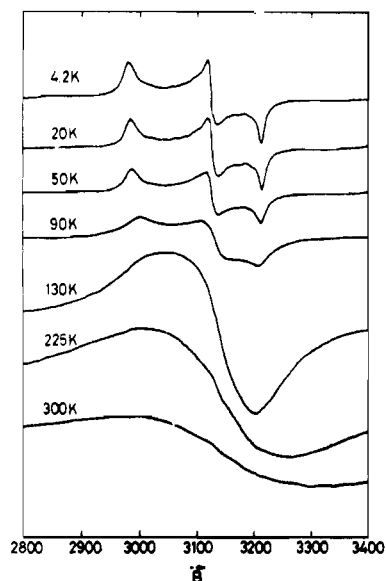


Figure 7. Temperature variation of the powder EPR pattern for (TMPD)Ni(mnt)₂.

Table VIII. Principal ESR Values of (TMPD)⁺Ni(mnt)₂⁻ in Solution, as a Powder, and as a Crystal and Comparison with Those of the Isolated Case

| system | g parameters | ref |
|---|--|-----------|
| (TMPD) ⁺ Ni(mnt) ₂ ⁻ | $g(\text{TMPD}^+) = 2.003$ | this work |
| acetone solution, 300 K | $g(\text{Ni}(\text{mnt})_2^-) = 2.066$ | |
| frozen solution, 77 K | $g_1 = 2.165, g_2 = 2.035,$ $g_3 = 1.998$ | |
| powder, 300 K | single broad line, $g = 2.03$ | |
| powder, 4.2 K | $g_1 = 2.145, g_2 = 2.046,$ $g_3 = 1.991$ | |
| single cryst, 77 K | $g_x = 2.140, g_y = 2.060,$ $g_z = 1.991$ | |
| Ni ³⁺ /(NBu ₄)Cu(mnt) ₂ | $g_x = 2.160, g_y = 2.040,$ $g_z = 1.998$ | 27 |

the interesting feature of the solution spectrum is the large line width (35 G) of the (TMPD)⁺ signal with the total loss of hyperfine structure while the Ni(mnt)₂⁻ signal is 18 G wide in comparison to 17 G for N(C₂H₅)₄Ni(mnt)₂ in acetone. This can only be explained by the formation of self-aggregates between (TMPD)⁺ units.

The frozen-solution spectra at 77 K in acetone yield a three-*g* pattern corresponding almost exactly to the principal values of pure N(C₄H₉)₄Ni(mnt)₂ in acetone. There is no resonance corresponding to (TMPD)⁺. This is however, understandable as even in pure (TMPD)⁺ClO₄⁻ the intensity of the EPR signal almost vanishes as the solution in acetone is cooled to 77 K due to dimer formation.²⁶

(ii) Powder Data. The powder exhibits a single broad line of ~350 G width at X-band at 300 K, which sharpens as the temperature is lowered. At these high temperatures down to 130 K, the single line is centered at $g = 2.03$, which is the average of the individual g_{av} 's of the two ions. At around 120–130 K, the single broad line splits into the familiar orthorhombic *g* pattern (Figure 7) whose principal values are close to but do not exactly match those of isolated Ni(mnt)₂⁻. The values are set out in Table VIII. Below 90 K down to 4 K there is a small but not insignificant change in the line width and the principal values. The ΔH_{pp} vs. *T* and g_{av} vs.

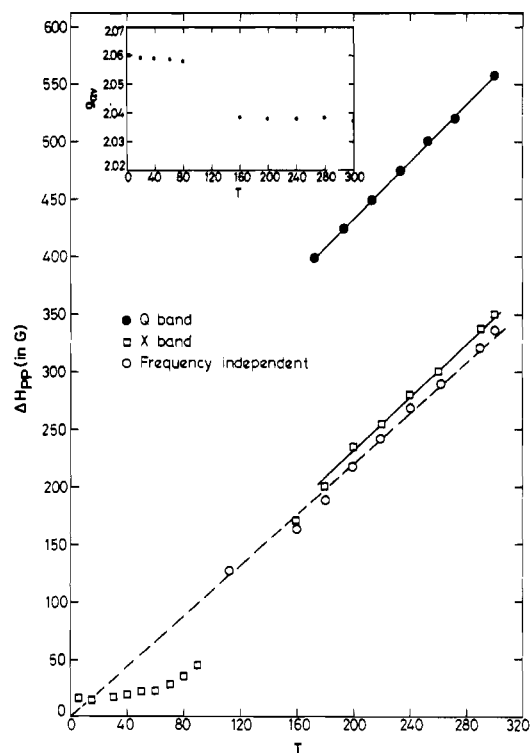


Figure 8. Temperature variation of line width of the powder at X and Q bands. In the inset is shown the variation of g_{av} .

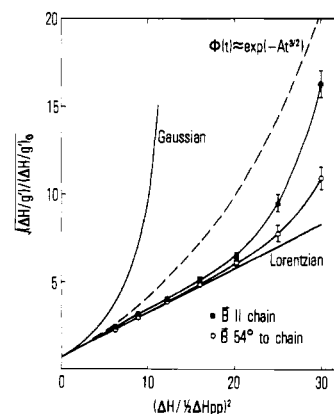


Figure 9. Line shape analysis at \vec{B} parallel to the chain axis and at the magic angle for (TMPD)Ni(mnt)₂ compared with Lorentzian, Gaussian, and 1-D line shapes.

T plots for the entire temperature range are shown in Figure 8.

The ion-radical salt, being formulated as [(TMPD)⁺[Ni(mnt)₂]⁻], in the absence of spin exchange interaction would yield a rhombic spectrum due to Ni(mnt)₂⁻ superimposed with a sharp line at $g = 2.003$ due to (TMPD)⁺. The lack of this type of spectrum implies that (a) no (TMPD)⁺ spins are present, (b) the (TMPD)⁺ resonance is not detectable due to the existence of a fast spin-lattice relaxation rate on that stack, or (c) spin exchange interactions are responsible for the observed spectrum. Argument (a) cannot account for the temperature dependence of the *g* values and (b) can be ruled out as such a fast relaxation rate requires metallic behavior from the stack, which is not observed.

Thus, the natural explanation for the temperature dependence of *g* is that there is rapid spin exchange between dissimilar systems whose contributions to susceptibility have different temperature dependences.

(iii) Line Shape Analysis. The line shape analysis for the $H || a$ and H at a 55° angle to *a* orientations revealed that it

(26) Thomas, D. D.; Keller, H. J.; McConnel, H. M. *J. Chem. Phys.* **1963**, *39*, 2321.

(27) Maki, A. H.; Edelstein, N.; Davison, A.; Holm, R. H. *J. Am. Chem. Soc.* **1964**, *86*, 4580.

is almost Lorentzian in character (Figure 9) at least near the center, with the $H\parallel a$ line being more non-Lorentzian.

(iv) **Frequency Dependence of Line Width.** The Lorentzian line shape indicates that the interaction rate between the TMPD⁺ and Ni(mnt)₂⁻ stacks is in either the fast or the slow limit as compared to the differences in the respective Larmor frequencies. If we assume a strong coupling limit, one would expect a decreasing line width with decreasing temperature, as T_2 increases as the temperature is lowered. The experimental observation agrees with the above although there are two temperature regions, where the slopes of the ΔH_{pp} vs. T curves are different.

The line width for the two-spin system in general is given by²⁸

$$\frac{1}{T_2} = \frac{\alpha_{\text{TMPD}}}{T_2(\text{TMPD})} + \frac{\alpha_{\text{Ni}}}{T_2(\text{Ni})} + \beta_{\text{TMPD-Ni}}(\nu_{\text{TMPD}} - \nu_{\text{Ni}})^2 \quad (2)$$

where T_2 's are the transverse relaxation rates for the respective stacks, $\beta_{\text{TMPD-Ni}}$ is the interaction term between the stacks, and α_{TMPD} and α_{Ni} are the respective fractions of the total χ on each type of stack. The frequency dependence of the line width will dictate whether the $\beta_{\text{TMPD-Ni}}(\nu_{\text{Ni}} - \nu_{\text{TMPD}})^2$ term is important or not.

A value for the interaction coupling $J'(T)$ can be evaluated from the differences in the X- and Q-band line widths at any temperature by using the formula²⁹

$$\Delta H_{Q-X}(T) = \frac{(\Delta g)^2 \beta^2}{Z(J'(T)h)^2} (H_Q^2 - H_X^2) \quad (3)$$

where Δg is the difference in the g_{av} 's of the two moieties and H_Q and H_X are the respective Zeeman fields for Q- and X-bands. With ΔH_{Q-X} given in MHz, the value of $J'(300)$ turns out to be 216 MHz (77 G) with Z being taken as 8. The large value of $|\nu_{\text{TMPD}} - \nu_{\text{Ni}}|$ explains the sizable difference in the X- and Q-band line widths albeit the small value of J' . Also in Q-band the three- g -value pattern separates out at a higher temperature (~ 130 K) than at X-band (~ 90 K).

The constant value of $\Delta H_Q - \Delta H_X$ over the temperature range 300–150 K shows that J' is nearly independent of T in this region. If the H_{Zee}^2 dependence on the line width is assumed, a frequency-independent line width ΔH_0 can be evaluated according to

$$\Delta H_0 = \frac{p^2(\Delta H_X) - \Delta H_Q}{p^2 - 1} \quad (4)$$

where $p = \nu_Q/\nu_X$. At 300 K, the ΔH_0 value is found to be 335 G. The temperature dependence of this frequency-independent line width is also shown in Figure 8 by the dashed line.

(v) **Decomposition of Susceptibility Contribution.** We assume that the magnetic susceptibility arises from the sum of the contributions of TMPD⁺ and Ni(mnt)₂⁻ spins. This is valid if exchange is not sufficiently large enough to lead to ferro- or antiferromagnetism.

For this purpose two temperature regions are to be recognized as with χ , (a) $T < 100$ K and (b) $T > 100$ K. A great deal of understanding has come about by the effort to determine the relative contribution of D⁺ and A⁻ stacks to a variety of physical properties such as magnetic susceptibility, electrical conductivity, etc. But there has been some doubt as to the choice of the g values to be used for the individual stacks and applicability to compounds with large interstack interaction.³⁰ However, these doubts are cleared in a later paper by Tomkiewicz.³¹ In the strong-coupling limit, where

Table IX. Variation of the Principal Values of the g Tensor^a and the Fraction (α_{Ni}) of the Total χ from the Ni(mnt)₂⁻ Stack with Temperature

| temp, K | g_1^b | g_3^b | α_{Ni}^c |
|---------|---------|---------|------------------------|
| 90 | 2.1335 | 1.9921 | 0.831 |
| 80 | 2.1346 | 1.9918 | 0.842 |
| 60 | 2.1400 | 1.9909 | 0.873 |
| 50 | 2.1406 | 1.9904 | 0.878 |
| 40 | 2.1414 | 1.9900 | 0.882 |
| 28 | 2.1416 | 1.9897 | 0.883 |
| 20 | 2.1421 | 1.9897 | 0.886 |
| 14.8 | 2.1423 | 1.9896 | 0.888 |
| 9.2 | 2.1429 | 1.9897 | 0.891 |
| 4.2 | 2.1451 | 1.9898 | 0.905 |

^a The g_2 value cannot be accurately evaluated. ^b The g values are accurate within ± 0.0010 . ^c The α value is calculated from g_1 values as described in the text.

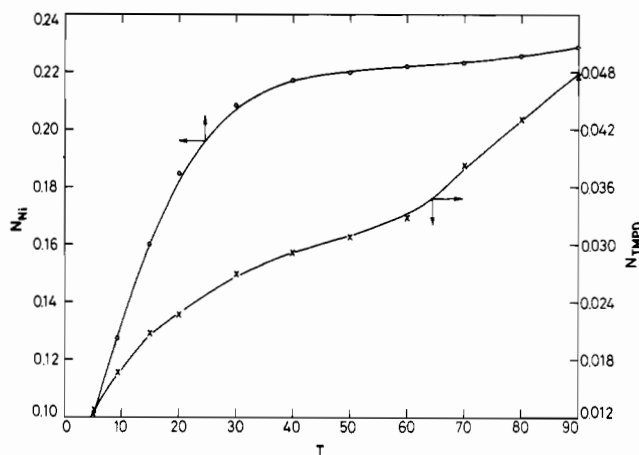


Figure 10. Fraction of the Ni(mnt)₂⁻ and TMPD⁺ spins contributing to susceptibility in the $T < 100$ K region. While N_{Ni} tapers off at 0.23, the TMPD⁺ fraction keeps on increasing monotonically.

the magnetic excitations on both the stacks are coherently mixed, the g tensor can be decomposed as

$$g(\theta, T) = (\alpha_{\text{Ni}}(T))(g_{\text{Ni}}(\theta)) + [1 - \alpha_{\text{Ni}}(T)](g_{\text{TM}}(\theta)) \quad (5)$$

where $\alpha_{\text{Ni}}(T)$ is the fraction of the susceptibility residing on Ni(mnt)₂⁻ at a temperature T and is given by

$$\alpha_{\text{Ni}}(T) = \frac{\chi_{\text{Ni}}(T)}{\chi_{\text{TMPD}}(T) + \chi_{\text{Ni}}(T)} \quad (6)$$

Rearranging eq 5, we get

$$\alpha_{\text{Ni}}(T) = \frac{|g_{\text{TM}}(\theta) - g(T, \theta)|}{|g_{\text{TM}}(\theta) - g_{\text{Ni}}(\theta)|} \quad (7)$$

As in the above expression we have used small differences in two large numbers, it is very critical that we choose the correct g 's for the calculation. Hence, g_1 values that are far removed from g_{TMPD} are chosen for accurate determination of α . Table IX shows the variation of g and α_{Ni} with temperature, and it is clear that the g_{max} value does not reach 2.160, which is the value in the isolated Ni(mnt)₂⁻, even at the lowest temperatures. This means that the spins are not entirely on Ni(mnt)₂⁻ and that a nonnegligible contribution of about 10% to α comes from the TMPD⁺ stack.

The effective number of spins per formula unit at any temperature due to each species can be obtained from

$$\frac{\chi_{\text{M}}(T + \theta)}{C} = (N_{\text{Ni}}g_{\text{Ni}}^2 + N_{\text{TMPD}}g_{\text{TMPD}}^2)/4 \quad (8)$$

(28) Tomkiewicz, Y.; Scott, B. A.; Tao, L. J.; Title, R. S. *Phys. Rev. Lett.* **1974**, *32*, 1363.

(29) McGregor, K. T.; Soos, Z. G. *Inorg. Chem.* **1976**, *15*, 2159.

(30) Conwell, E. *Phys. Rev. B: Condens. Matter* **1980**, *22*, 3107.

(31) Tomkiewicz, Y.; Taranko, A. R.; Torrance, J. B. *Phys. Rev. B: Condens. Matter* **1980**, *22*, 3113.

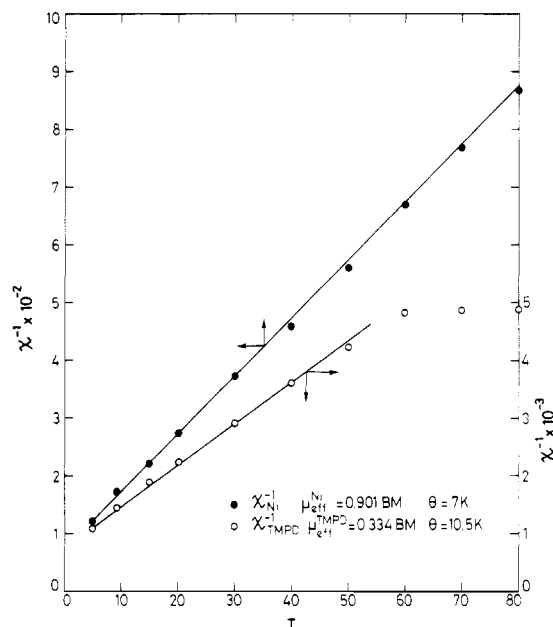


Figure 11. Decomposition of the susceptibility into contributions from the TMPD^+ and $\text{Ni}(\text{mnt})_2^-$ stacks.

where N_{Ni} and N_{TMPD} are the number of spins per $\text{Ni}(\text{mnt})_2^-$ and TMPD^+ , respectively. It is required that both spin susceptibilities follow a simple Curie-Weiss law behavior, for the above relation to hold. The temperature variation of N_{Ni} and N_{TMPD} is shown in Figure 10.

Now the individual contributions can be separated by using

$$\chi_{\text{Ni}} = N_{\text{Ni}} \frac{C_{\text{Ni}}}{T + \theta} \quad (9)$$

where

$$C_{\text{Ni}} = \frac{g_{\text{Ni}}^2 \beta^2 N_0}{4k}$$

and $\chi_{\text{TMPD}} = (\chi_{\text{total}} - \chi_{\text{Ni}})$.

The χ_{Ni}^{-1} vs. T plot (Figure 11) follows a Curie-Weiss behavior in the low-temperature range with a Curie constant $C_{\text{Ni}} = 0.1015 \text{ mol}^{-1}$, which yields $\mu_{\text{eff}}(\text{Ni}) = 0.901 \mu_{\text{B}}$ and a Weiss constant $\theta = 6 \text{ K}$. The χ_{TMPD}^{-1} vs. T plot (in Figure 11) also follows the Curie-Weiss law with $C = 0.014 \text{ mol}^{-1}$, $\mu_{\text{eff}} = 0.334 \mu_{\text{B}}$, and $\theta = 10.5 \text{ K}$.

The reduced susceptibility of the metal chelate system must result from strong exchange interactions which lead to a singlet ground state, and the contribution to paramagnetism has to arise from defect sites that are not so strongly coupled to the rest. This type of behavior has been observed in (perylene) $_2^+\text{Pd}(\text{mnt})_2^-$ ¹³ also. The X-ray structure, which could not be refined further than $R = 9.8\%$ is also indicative of a solid with a large degree of disorder. But the value of 23% of $\text{Ni}(\text{mnt})_2^-$ at defect sites, as observed from the temporary variations of N_{Ni} , is rather large.

A similar g value decomposition is not possible in the high-temperature region (100–300 K) as the EPR spectrum consists of a single broad line and not the rhombic g pattern of the low-temperature region. The broad line occurs at $g = 2.030$, which is the average of the g_{iso} 's of the component ions, and its g is temperature independent in the high-temperature region.

(vi) Temperature Dependence of Line Width of Powder.

Figure 8 shows the ΔH_{pp} vs. T plot for the powder from 4 to 300 K at X-band and 110 to 300 K for Q-band. Due to the large value of the exchange parameter, the high-temperature second moment is expected to be given by mainly the anisotropic exchange term^{29,32} D_e (which is of the order $(\Delta g/g)^2 J_0$

and the dipolar and hyperfine contributions can be neglected. Thus in the high-temperature approximation $kT \gg J_0$ of the Blume-Hubbard model³³ Γ can be written as

$$\Gamma = (\frac{3}{2})^{1/2} (\Delta H_{\text{pp}}) = (\frac{3}{2})^{1/2} D_e^2 / J_0 \quad (10)$$

Equation 9 has to be modified for the $kT \leq J_0$ region (which is the case for $T < 90 \text{ K}$ in $(\text{TMPD})\text{Ni}(\text{mnt})_2$), and as a rigorous treatment is rather difficult, we have resorted to the approximate expressions given by McGregor and Soos.²⁹ The line width becomes temperature dependent in this region and is given by

$$\Delta H_{\text{pp}}(T) = 2[6^{1/2} D_e^2 (\rho(T)) / 3J_0] \quad (11)$$

where $\rho(T)$ is the effective density of spins, which for a regular 1-D Heisenberg chain is given by

$$\rho_{\text{H}}(T) = 4x(f(x)) \quad (12)$$

with $x = kT/J_0$ and $f(x)$ values tabulated by Bonner and Fisher³⁴ ($f(x)$ varies between 0.05 and 0.07 for $x = 0-2.5$).

As has been discussed earlier in section 3D(iii), despite the presence of two chains whose g tensors are different, $(\text{TMPD})\text{Ni}(\text{mnt})_2$ yields a single exchange-narrowed line due to an interchain interaction J' with Z neighboring chains. Hence, the total expression for the temperature variation of ΔH_{pp} is

$$\Delta H_{\text{pp}}(T) = A(\rho(T)) + B H_0^2 (\rho^{-1}(T)) \quad (13)$$

where $A = 2(6^{1/2} D_e^2 / 3J_0)$ and $B = (g_1 - g_2)^2 \beta^2 / ZJ'h^2$. Using the frequency-independent line width shown in Figure 8, one can get an idea of D_e and J_0 . The slope of the curve gives D_e/J_0 to be 1.94×10^{-2} , which is about an order of magnitude larger than what is expected from a simplistic picture³² of $(\Delta g/g)^2$ (approximately 10^{-3}). Such large ratios of D_e/J are quite commonly encountered in the literature in systems studied earlier.

(vii) Single-Crystal EPR. (a) g Tensor. The principal values and their direction cosines are the two aspects of the g tensor which can throw some light on the interactions of the paramagnetic species with its surroundings. In the particular case of $(\text{TMPD})\text{Ni}(\text{mnt})_2$, both ions are paramagnetic and also there is the possibility of charge transfer from TMPD^+ to $\text{Ni}(\text{mnt})_2^-$ as evidenced from crystal structure. To our knowledge there has been no attempt so far at a systematic correlation of EPR spin Hamiltonian parameters with the degree of charge transfer in ion-radical salts. However, in regular chain compounds with magnetically inequivalent chains such as TMPD -chloranil and p -phenylenediamine-chloranil³⁶ temperature-dependent shifts of the g tensor direction cosines from the molecular axes have been observed and accounted for by Soos^{37,38} in terms of delocalization of the excitons between inequivalent chains by means of interchain dipolar coupling. The 77 K diagonalized g values (Table IX) are different from the $\text{Ni}(\text{mnt})_2^-$ value, and the reason has already been given for this temperature-dependent shift of g values. In our single-crystal study, we have attempted to analyze the spectrum when $B \parallel a$ and B is in a plane perpendicular to the "a" axis as the crystals obtained were rather small needles whose needle axis could be positively identified as the "a" axis. The g value for $B \parallel a$ was experimentally found to be 1.998, whereas the value predicted with use of the direction cosines

(32) Moriya, T. *Phys. Rev.* **1960**, *120*, 91.

(33) Blume, M.; Hubbard, J. *Phys. Rev. B: Solid State* **1970**, *1*, 3815.

(34) Bonner, J. C.; Fisher, M. E. *Phys. Rev.* **1964**, *135*, A640.

(35) Hughes, R. C.; Soos, Z. G. *J. Chem. Phys.* **1968**, *48*, 1066.

(36) Poit, G. T.; Kommandeur, J. *Mol. Phys.* **1967**, *13*, 373.

(37) Soos, Z. G. *J. Chem. Phys.* **1968**, *49*, 2493.

(38) Strelbel, P. J.; Soos, Z. G. *J. Chem. Phys.* **1969**, *50*, 2911.

from the crystal structure is 2.036. Also the simulated g value for the a axis rotation does not match the experimental variation if the direction cosines from the crystal structure are used. Hence we conclude that in (TMPD)Ni(mnt)₂ the g tensor direction does not correspond to the Ni(mnt)₂⁻ molecular framework. The best fit was obtained if the minimum g was assumed to be almost along the a axis, which is also the stack axis, this making an angle of $\sim 35\text{--}40^\circ$ with the normal to the Ni(mnt)₂⁻ plane.

We have no satisfactory explanation for this shift, but we feel it is due to the charge-transfer interaction between the two moieties. Further, from a molecular model of the unit cell it is quite evident that the various short contact vectors between TMPD⁺ and Ni(mnt)₂⁻ lie along the " a " axis and hence the orbital overlap pathway is along " a ", the stack axis.

(b) **Line Width.** The g tensor at 77 K closely resembles that of Ni(mnt)₂⁻ in its principal values, and hence for the calculations of the line width variation a reference spin " in " is chosen on that stack. The total spin Hamiltonian can be written as

$$\mathcal{H} = \sum (\beta B \cdot g_{in} S_{in} + S_{in} D_{ii} S_{in+1} - 2J_{ii} S_{in} S_{in+1}) + (S_{in} D_{ij} S_{jn} - 2J_{ij} S_{in} S_{jn}) + (\beta \cdot B \cdot g_{jn} S_{jn} + S_{jn} D_{jj} S_{jn+1} - 2J_{jj} S_{jn} S_{jn+1}) \quad (14)$$

where i and j refer to Ni(mnt)₂⁻ and TMPD⁺ stacks, respectively, D_{ii} and D_{jj} contain both dipolar and anisotropic exchange parts, J_{ii} and J_{jj} are the isotropic exchange parameters of the Ni(mnt)₂⁻ and TMPD⁺ stacks, respectively, and J_{ij} is the interchain exchange.

We will be neglecting J_{ij} and Zeeman, the dipolar and exchange Hamiltonians of the TMPD⁺ stack, for the analysis of line width.

We have followed the treatment of McGregor and Soos³⁹ in evaluating the line width variation in the plane perpendicular to the " a " axis by using the equation

$$\Delta H_{PP} = \frac{2(2^{1/2})}{3(3^{1/2})} \frac{1}{J_{ii}} \{M_2^D + \rho(M_2^D(0))\} \quad (15)$$

where ΔH_{PP} is the peak to peak width of the derivative line, M_2^D is the total second moment arising out of both dipolar and anisotropic exchange contributions, and $M_2^D(0)$ is the only secular part which gets enhanced due to the low dimensionality, with ρ , the dimensionality determining the enhancement. (ρ values on the order of unity can be used because the degree of 1-D character is not large as evidenced by the nearly Lorentzian line shape in the plane perpendicular to a .)

Equation 15 is rewritten in terms of the various variables ρ , D_e and J (a short analysis of the equation is given in Appendix B):

$$\Delta H_{PP} = \frac{C_1[D_e^2(C_2 + \rho C_3) + D_e(C_4 + \rho C_5) + \rho C_6 + 1]}{J_{ii}} \quad (16)$$

The simulated curves for the various values of J_{ii} , D_e , and ρ along with the experimental variation in the plane perpendicular to a are shown in Figure 12. The experimental line width at $B \parallel a$ could not be analyzed in the above manner as the line shape is not Lorentzian as expected for a low-dimensional system when the magnetic field vector is along the chain axis.

As seen in Figure 12, there is no unique set of J_0 , D_e , and ρ that matches the experimental value and the variation. J_0 ranging from 15 to 4.5 cm⁻¹, D_e ranging from 0.3 to 0.09 cm⁻¹, and ρ ranging from 1 to 8 give a reasonable fit of the experimental curve.

The lower values of J obtained from the EPR line width fitting procedure yields values of ϵ , which is in fact the ratio

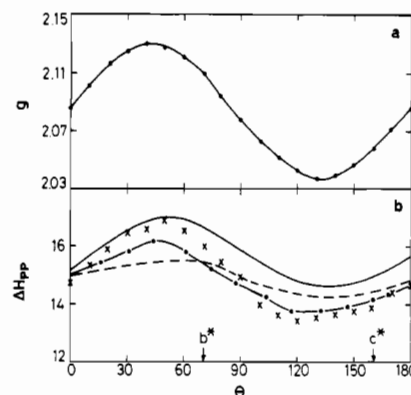


Figure 12. (a) Experimental g variation and (b) ΔH_{PP} variation (\times) in the plane perpendicular to the " a " axis. The values are calculated from eq 16 with use of the following values: (—) $J_0 = -4.5 \text{ cm}^{-1}$, $D_e = -0.09 \text{ cm}^{-1}$, $\rho = 8$; (---) $J_0 = 15 \text{ cm}^{-1}$, $D_e = -0.8 \text{ cm}^{-1}$, $\rho = 1$; (-O-) $J_0 = -6.5 \text{ cm}^{-1}$, $D_e = -0.13 \text{ cm}^{-1}$, $\rho = 5$.

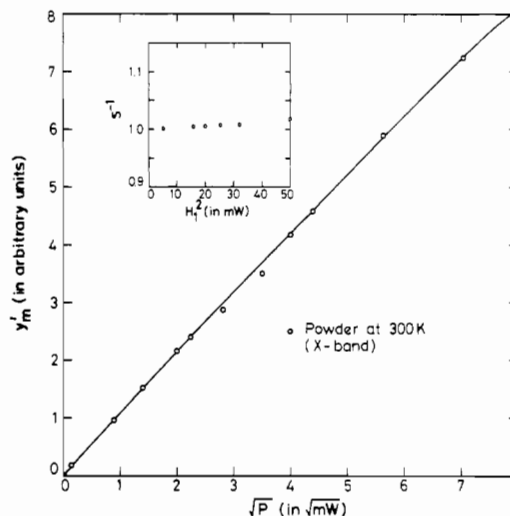


Figure 13. Variation of derivative amplitude with the square root of power. This yields a straight line, thus showing that there is no saturation. In the inset is the variation of the saturation parameter, which also confirms this.

between the exchange between segments and within segments, between 0.125 (for $J_0 = 15 \text{ cm}^{-1}$) and 0.035 (for $J_0 = 4.5 \text{ cm}^{-1}$). Then this is in general agreement with the earlier prediction that the EPR signal below 90 K is from the Ni(mnt)₂⁻ odd chain segments which are not as strongly coupled with other such segments as within themselves.

(viii) **Spin-Spin and Spin-Lattice Relaxation.** Since the EPR lines are nearly Lorentzian, the spin relaxation behavior may be described by using Bloch equations.⁴⁰ Thus

$$\frac{1}{T_2} = g(\Delta H_{PP})(7.616 \times 10^6) \text{ s}^{-1}$$

At 300 and 200 K we obtain T_2 's of 1.93×10^{-10} and 3.065×10^{-10} s, respectively. For the sake of comparison the T_1 and T_2 values of (TMPD)ClO₄⁴¹ and (TMPD)TCNQ⁴² are given

$$\begin{array}{l} \text{(TMPD)ClO}_4 \\ T_1 = 6 \times 10^{-8} \text{ s} \quad T_2 = 3 \times 10^{-7} \text{ s} \\ \text{(TMPD)TCNQ} \\ T_1 = 1.5 \times 10^{-6} \text{ s} \quad T_2 = 3 \times 10^{-7} \text{ s} \end{array}$$

(40) Poole, C. P. "Electron Spin Resonance"; Interscience: New York, 1967; p 705.

(41) Goldsborough, J. P.; Mandel, M.; Pake, G. E. *Phys. Rev. Lett.* **1960**, *4*, 13.

The spin-lattice relaxation rates $1/T_1$ can be obtained by progressive saturation of the ESR line. For a spin system with a Lorentzian line shape, a plot of the derivative amplitude against the square root of power should yield a straight line if the signal does not saturate at available powers. Figure 13 shows such a plot, and we see that γ'/H_1 is nearly constant for available powers in the spectrometer.

The saturation parameter S can be evaluated by using

$$S^{-1} = [\lim_{H_1 \rightarrow 0} (\gamma'/H_1) / (\gamma'/H_1)]^{2/3} \\ = 1 + H_1^2 \gamma^2 T_1 T_2$$

If we take $H_1 = 0.1$ G (typical for the EPR experiment) and $\gamma = 10^7$ rad G⁻¹, we find that saturation sets in⁴³ when $\gamma^2 H_1^2 T_1 T_2 \approx 1$, for (TMPD)Ni(mnt)₂, and this happens only if $T_1 > 10^{-2}$ s.

The plot of S^{-1} vs. H_1^2 (in mW) is shown in the inset of Figure 13, and this clearly shows that the variation in S^{-1} is almost negligible and hence determination of T_1 by this method is difficult. That systems having large J possess an exchange lattice relaxation much faster than the direct Zeeman lattice relaxation indicates that T_1 is small. Only a temperature variation of T_1 would give us some idea of the mechanisms responsible for relaxation. Hence at the present we cannot say much about T_1 except that both T_2 and T_1 are expected to be smaller than in similar systems such as (TMPD)TCNQ (where exchange participation is present) due to the larger spin-orbit coupling.

4. Conclusions

The two units form segregated stacks along the "a" axis. The various short contacts between the two moieties and the long C≡N bond length indicate charge transfer from TMPD⁺ to Ni(mnt)₂⁻. The analysis showed that there is disorder, and this was later confirmed by magnetic studies.

The susceptibility studies show that there are two temperature regions—a Curie type behavior below 100 K, which can also be well described by a power law dependence arising from disorder, and an almost temperature-independent susceptibility above 100 K. Below 100 K the system can be described as an ensemble of disordered localized paramagnetic moments. The low value of $\mu_{\text{eff}} = 0.942 \mu_B$ is due to the strong exchange interaction present in the systems, and the paramagnetism arises from defect sites which are not strongly coupled to the neighbors. A value of exchange was found to be ~ 120 cm⁻¹ from the temperature dependence of χ . Decomposition of the susceptibility contributions indicates that about 83% comes from the Ni(mnt)₂⁻ stack at 90 K, and it increases to 90% at 4.2 K. Solution EPR shows that even though the ion-radical salt dissociates there is still some aggregate formation. Powder EPR results match well with the susceptibility studies. The frequency and temperature dependence of the powder line width yielded a value of D_c/J of 1.94×10^{-2} .

Single-crystal EPR studies yielded g -tensor direction cosines that do not coincide with molecular directions of the Ni(mnt)₂⁻ ion but rather are crystallographic. The g_z (1.992) direction is tilted by about 40° from the normal to the Ni(mnt)₂⁻ plane toward the "a" axis. The line width analysis in a plane perpendicular to "a" was carried out to give values of J , D_e , and ρ of -15 to -4.5 cm⁻¹, -0.30 to -0.09 cm⁻¹, and 1–8, respectively. The weaker exchange, ϵJ_0 , between the odd segments responsible for EPR is thus obtained to be 0.1 J , and the concentration of these segments is obtained to be 0.23 from the susceptibility studies. The line shape analysis at $B \parallel$ "a" showed that the system is quite one-dimensional, whereas at

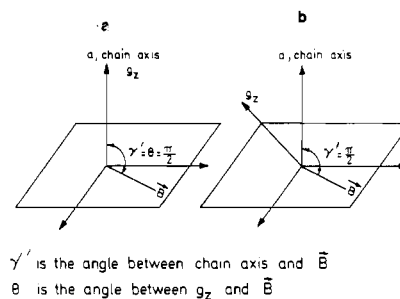


Figure 14. Two coordinate systems for (TMPD)Ni(mnt)₂: (a) g_z direction along the chain axis; (b) g_z direction along the perpendicular to the Ni(mnt)₂⁻ plane as determined by crystallography.

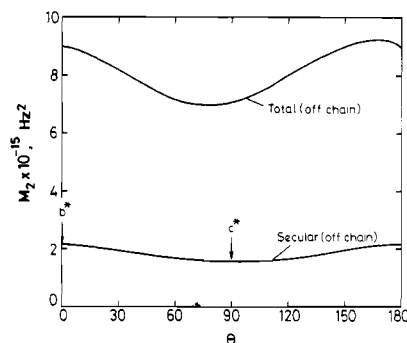


Figure 15. Off-chain dipolar contribution in the plane perpendicular to the "a" axis.

$B \perp$ "a", a nearly Lorentzian line shape was observed.

The signal does not saturate at available powers, and hence a value of T_1 could not be obtained. However, due to the participation of exchange in the relaxation processes T_1 is expected to be small.

Acknowledgment. B.L.R. is grateful to the Department of Atomic Energy for assistance in the form of a Research Fellowship. We are thankful to Dr. G. V. N. Appa Rao for help in obtaining the ORTEP diagrams and to G. V. R. Chandramouli for assistance in writing the computer program for the fitting of line width.

Appendix A

The structure was solved by the usual heavy-atom methods by the combination of Patterson, Fourier, and least-squares analysis. The Ni atom was placed at (0, 0, 0), and the three-dimensional Patterson map was calculated by using eq A-1. The strongest peaks gave the location of S . Refinement

$$P(u, v, w) = \sum_{h=0}^{h_{\text{max}}} \sum_{k=0}^{k_{\text{max}}} \sum_{l=0}^{l_{\text{max}}} I(hkl) \cos(2\pi hu) \cos(2\pi kv) \cos(2\pi lw) \quad (\text{A-1})$$

followed by a difference Fourier synthesis revealed the positions of all the non-hydrogen atoms. The calculations were performed on a IBM 370/155 computer at the IIT Madras Computer Centre using the SHELX-76 program for crystal structure determination.⁴⁴ The function minimized was

$$\sum w_{hkl} (|F_o| - |F_c|)^2$$

where F_o and F_c are the observed and calculated structure factors and w_{hkl} is the relative weight of a reflection.⁴⁵ The atomic scattering factors were taken from Cromer and Mann.⁴⁶ Anomalous dispersion correction factors were obtained from Cromer and Liberman.⁴⁷ Anisotropic thermal factors were

(42) Hoffman, B. M.; Hughes, R. C. *J. Chem. Phys.* **1970**, *52*, 4011.

(43) Abragam, A.; Bleaney, B. "Electron Paramagnetic Resonance of Transition Ions"; Clarendon Press: Oxford, 1970; p 119.

(44) Sheldrick, G. M. "Shelx-76", University of Cambridge, Cambridge, England, 1976.

(45) Stout, G. H.; Jensen, L. H. "X-ray Crystal Structure and Determination—A Practical Guide"; Macmillan: London, 1968.

(46) Cromer, T.; Mann, I. B. *Acta Crystallogr., Sect. A* **1968**, *24*, 321.

(47) Cromer, D. T.; Liberman, J. *J. Chem. Phys.* **1970**, *53*, 1891.

assigned to all non-hydrogen atoms.

The final disagreement factor defined as $R = \sum |F_o| - |F_c| / |F_o|$ obtained was 0.094. Disorder in the TMPD unit hampered further refinement of the R factor. The hydrogen atoms could not be located from the final difference Fourier maps. There seems to be quite a bit of thermal disorder among the two ion radicals as indicated by the numerous correlation matrix elements (>0.5) obtained during least squares after introduction of the anisotropic thermal parameters. There is also evidence for a large degree of disorder from susceptibility data.

Appendix B

Figure 14 gives two coordinate systems for (TMPD)Ni(mnt)₂. The secular and nonsecular contributions from all the neighbors except the two on the chain vary as shown in Figure

15. As is seen, the secular part is much less and unless the system is highly one-dimensional (i.e. $\rho \gg 1$) it does not contribute substantially. The off-chain contributions were found to be affected only negligibly by the change in the direction cosines of the g tensor.

On the other hand, contributions from the two neighbors on the Ni(mnt)₂⁻ stack are very sensitive to the orientation of the g tensor and the better fit was obtained only when the g_z direction was taken to be along "a", the stack axis. Both positive and negative values of D_e were tried, and the angular variation was better predicted by taking D_e to be negative. The value of ρ indicates the system is quite low dimensional, which is in agreement with the non-Lorentzian line shape observed for $B||$ chain axis.

Registry No. (TMPD)Ni(mnt)₂, 85762-15-8.

Contribution from the Istituto Chimica Generale, Facoltà di Farmacia, University of Florence, and ISSECC, CNR, Florence, Italy

π -Bonding Interactions of Nonlinearly Ligating Ligands with Octahedral Cobalt(II) Complexes

A. BENCINI,^{1b} C. BENELLI,^{1a} D. GATTESCHI,^{*1a} and C. ZANCHINI^{1a}

Received May 19, 1982

The EPR spectra of several trigonal-octahedral cobalt(II) complexes have been used to obtain information on the π -bonding anisotropic interactions. The pattern of g values is strongly influenced by the difference between the two π -bonding parameters of individual ligands in the angular-overlap model. It was found that in CoO₆ chromophores the larger π interaction is orthogonal to the Co-O-R plane. For CoN₆ chromophores, where N is provided by imidazoles or bipyridine, no evidence of dominant π back-bonding was found, in agreement with previous findings.

In recent years there has been a systematic attempt to investigate low-symmetry components of the ligand field, thanks to the development of the angular-overlap model, AOM.²⁻⁶ As a matter of fact the use of this model gives an effective parameterization of low-symmetry fields by using parameters that are in principle related to the σ - and π -donor ability of the atoms surrounding a central metal ion.² It is now currently believed that the values of the parameters obtained from the analysis of several spectroscopic and magnetic data do reflect some chemical sense and that they can be transferred from one complex to another, provided that the necessary caution is observed.⁷

One of the fascinating fields of application of the angular-overlap model is that of the determination of anisotropic π components in the interaction of nonlinearly ligating ligands with transition-metal ions. In fact when the donor atom belongs to a molecule, the M-L moiety does not usually possess cylindrical symmetry so that it is generally to be expected that the π interaction with the metal ion is not isotropic. This has

Table I. Observed g and Calculated D^a and γ^a Values for Some Trigonal Cobalt(II) Complexes

| | D , cm ⁻¹ | γ | $g_{ }$ | g_{\perp} |
|---|------------------------|----------|----------|-------------|
| Co(H ₂ O) ₆ | 397 | -1.44 | 5.82 | 3.44 |
| Co(pyO) ₆ ^b | -652 | -1.16 | 2.26 | 4.77 |
| Co(apy) ₆ (ClO ₄) ₂ | -355 | -1.46 | 3.08 | 4.85 |
| Co(<i>N</i> -MeIz) ₆ ^c | -367 | -1.47 | 3.06 | 4.87 |
| Co(Iz) ₆ (NO ₃) ₂ | 323 | -1.38 | 5.55 | 3.53 |
| Co(en) ₃ (NO ₃) ₂ | -581 | -1.48 | 2.6 | 5.0 |
| Co(bpy) ₃ Br ₂ | -258 | -1.25 | 3.16 | 4.62 |

^a D and γ values are calculated as described in the text to reproduce the observed g values within ± 0.005 . ^b pyO is pyridine *N*-oxide. ^c *N*-MeIz is *N*-methylimidazole.

now been established in several cases, in which it was found that a good interpretation of the spectral and magnetic properties of the complexes⁹⁻¹¹ could not be achieved by considering the donor atoms as spherical.

Octahedral cobalt(II) complexes appear to be extremely well suited for recognizing π -bonding anisotropy, since low-symmetry components of the ligand field are easily monitored through the EPR spectra.^{12,13} In particular, trigonal com-

- (1) (a) University of Florence. (b) ISSECC, CNR.
- (2) Schäffer, C. E. *Struct. Bonding (Berlin)* **1968**, *5*, 68.
- (3) Gerloch, M.; McMeeking, R. F. *J. Chem. Soc., Dalton Trans.* **1975**, 443.
- (4) Horrocks, W. D.; Burlone, D. A. *J. Am. Chem. Soc.* **1976**, *98*, 6512.
- (5) Bertini, I.; Gatteschi, D.; Scozzafava, A. *Isr. J. Chem.* **1977**, *15*, 188.
- (6) Hitchman, M. A. *Inorg. Chem.* **1977**, *16*, 1985.
- (7) Bencini, A.; Benelli, C.; Gatteschi, D.; Zanchini, C. *Inorg. Chem.* **1980**, *19*, 1301.
- (8) Bencini, A.; Benelli, C.; Gatteschi, D.; Zanchini, C. *Inorg. Chem.* **1980**, *19*, 3027.

- (9) Mackey, D. J.; Evans, S. V.; McMeeking, R. F. *J. Chem. Soc., Dalton Trans.* **1978**, 160.
- (10) Byers, W.; Lever, A. B. P.; Parisch, R. V. *Inorg. Chem.* **1968**, *7*, 1835.
- (11) Carlin, R. L.; O'Connor, C. J.; Bathia, S. N. *J. Am. Chem. Soc.* **1976**, *98*, 685.
- (12) Bencini, A.; Gatteschi, D. *Transition Met. Chem.* **1982**, *8*, 1.
- (13) Banci, L.; Bencini, A.; Benelli, C.; Gatteschi, D.; Zanchini, C. *Struct. Bonding (Berlin)* **1982**, *52*, 37.